Dressing control of biphoton waveform transitions

Xinghua Li, Dan Zhang, Da Zhang, Ling Hao, Haixia Chen, Zhiguo Wang,* and Yanpeng Zhang*

Key Laboratory for Physical Electronics and Devices of the Ministry of Education & Shaanxi Key Lab of Information Photonic Technique, Xi'an Jiaotong University, Xi'an 710049, China

(Received 21 October 2017; published xxxxxx)

We experimentally realize and theoretically analyze narrow-band biphotons generated in a hot rubidium vapor cell by four-wave-mixing processing. A dressing laser beam is used to alternate both linear and nonlinear susceptibilities of the vapor, thereby modifying the biphoton's temporal correlation function. Most notably, the correlation time is increased from 6 to 165 ns. The biphoton shape is also shown to change as a result of the coupled-states dressing. We observed Rabi oscillations and optical precursors in hot atomic vapor cells. We also theoretically simulated biphoton correlation times as influenced by dressing-laser detuning and power, the results of which are consistent with our experiments.

DOI: 10.1103/PhysRevA.00.003800

I. INTRODUCTION

Entangled photon pairs are essential for fundamental tests of quantum mechanics [1] and optical quantum technologies [2–5]. The most widespread technique for creating these quantum resources is spontaneous parametric down-conversion (SPDC) of laser light into photon pairs [6]. However, these prepared biphotons typically have very wide bandwidths (>THz) and short coherence times (<ps), which make them extremely difficult for implementing photonic quantum information processing in an atomic-memory-based quantum network [7]. Many efforts have been made over the last decade in order to narrow down the SPDC photon bandwidth by using optical cavities [8–10]. A fully tunable, narrow-band, and efficient single-photon source was realized based on a whispering gallery mode resonator (WGMR) and demonstrating a tunability of bandwidth between 7.2 and 13 MHz [11]. More recently, coupling of alkali dipole transitions with a narrowband photon pair source is reported with a cavity in use [12]; this process discussed in more detail in Ref. [13]. However, the bandwidth of SPDC polarization-entangled photon pairs is still wider than most atomic transitions and leads to very low efficiencies in storing these polarization states in a quantum memory [9–14]. To solve this problem, four-wave mixing in a cold cesium atomic ensemble using the same levels configuration as in the present paper has already been used to control the biphoton wave shape [15]. Moreover, subnatural-linewidth biphotons with controllable waveforms have been produced from spontaneous four-wave mixing (SFWM) in cold atoms (10–100 μK) [16–20]. The phenomenon of Rabi oscillations was observed in a rubidium atomic ensemble by periodically modulating two input classical lasers [21]. However, all the results mentioned above were obtained from cold atom systems, which are very expensive and require complicated operations as well as a complex timing control with a low duty cycle [22]. By choosing hot atomic vapor cell systems to prepare narrowband biphoton, the system size and operation can be markedly simplified, resulting in significant cost savings. Shaping of few-photon sub-Poissonian light pulses was observed in a magnetically shielded ^{87}Rb vapor cell [23]. Recently, subnatural-linewidth biphotons have been generated in hot atom systems, assisted by paraffin coating and spatially separated optical pumping [24], and the biphoton generation process has been optimized by utilizing spatially tailored hollow beams for optical pumping [25].

In this paper, we prepare narrowband biphoton in double-Λ levels from a Doppler-broadened hot rubidium atomic vapor cell. Assisted by a dressing laser to control both spontaneous four-wave mixing nonlinear parametric interaction and linear interaction, we achieve biphoton correlation time ranging from 6 to 165 ns. The biphoton shape is also shown to change as a result of the coupled-states dressing. In addition, we simulate the variations of group delay bandwidth and nonlinear bandwidth with dressing field detuning and power, and the results coincide with our experiments.

The paper is organized as follows: In Sec. II, we present the experimental setup and basic theory of the dressing biphoton generation process. Section III presents the experiment results along with the theoretical simulation of the biphoton correlation time. In Sec. IV, we draw conclusions resulting from this work.

II. EXPERIMENTAL SETUP AND BASIC THEORY

The experimental setup and atomic energy-level diagrams are illustrated in Figs. 1(a) and 1(b), respectively. A thermal temperature-stabilized rubidium vapor cell with magnetic shielding of μ-metal has a longitudinal length $L = 5.5$ cm. In the presence of two counter-propagating cw beams termed the "pump" $\boldsymbol{E}_2$ (frequency ω_2) and "coupling" lasers $\boldsymbol{E}_1$ (frequency ω_1), paired spontaneous photons termed "Stokes" and "anti-Stokes" are generated in the atomic cloud and propagate in opposite directions along the z axis. To keep the parametric gain small, the linearly polarized pump beam is weak and 2.0 GHz detuned from the resonance transition $|0\rangle \rightarrow |2\rangle$. The intense coupling beam is also linearly polarized

*wangzg@mail.xjtu.edu.cn, ypzhang@mail.xjtu.edu.cn

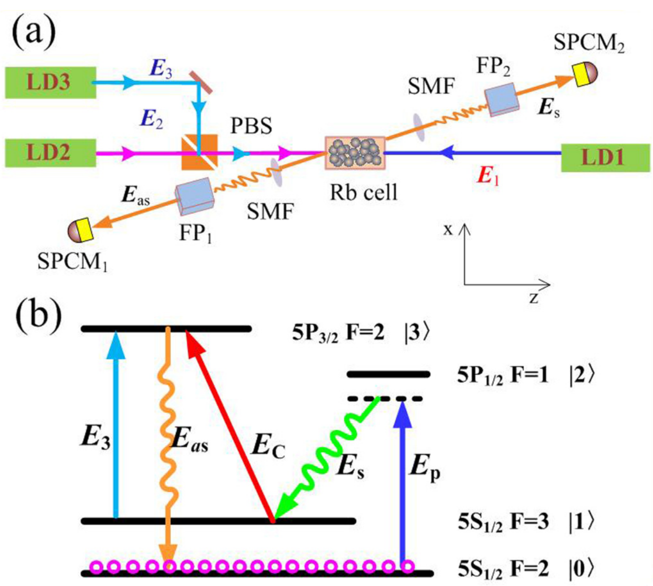

FIG. 1. (a) Alignment of spatial beams for biphoton-generation process. LD: external cavity diode lasers; PBS: polarization beam splitter, SPCM: single-photon counting module, SMF: single-mode fibers, FP: Fabry–Perot cavity. (b) Energy-level diagram for four-level configuration in ^{85}Rb vapor.

and tuned to resonance with the $|1\rangle \rightarrow |3\rangle$ transition to enhance the atom-field interaction and provide electromagnetically induced transparency (EIT) for the generated anti-Stokes photons. Another linearly polarized laser $\boldsymbol{E}_3$ (frequency ω_3) propagates in the same direction with the pumping laser and makes the $|1\rangle \rightarrow |3\rangle$ transition to modulate the rubidium atomic energy level. The phase-matched Stokes (ω_s) and anti-Stokes (ω_{as}) paired photons are propagating in opposite directions and with a 4° angle between the z axis in order to avoid the fluorescence-photon-counting effect. The paired photons are then coupled into two opposing single-mode fibers (SMFs), followed by Fabry–Perot cavity filters (500 MHz bandwidth), and detected by two single-photon counting modules (SPCMs). The biphoton coincidence counts are recorded by a time-to-digital converter using a temporal bin width of 0.0244 ns.

According to perturbation theory, the interaction of the Hamiltonian describes the four-wave mixing process and determines the evolution of the two-photon state vector [26]. This gives a clear picture of the biphoton generation mechanism [27]. Here, the two-photon amplitude in the time domain is represented by

$$\psi(\tau) = \frac{L}{2\pi} \int d\omega_{as} \kappa(\omega_{as}) \Phi(\omega_{as}) e^{-i\omega_{as}\tau}, \tag{1}$$

where $\Phi(\omega_{as})$ is defined as the longitudinal detuning function $\Phi(\omega_{as}) = \mathrm{sinc}(\frac{\Delta k L}{2}) e^{i\frac{L}{2}[k_s(\omega_s)+k_{as}(\omega_{as})]}$, $k_{s,\,as}$ are wavenumbers of Stokes and anti-Stokes photons, $\Delta k = k_{as} + k_s - (k_c + k_p)$ is the phase mismatching for our energy configurations, the relative time delay τ is defined by $\tau = t_{as} - t_s$, and L is rubidium medium length. From Eq. (1), we obtain that the biphoton wave function is determined by both the nonlinear coupling coefficient κ and the longitudinal detuning function. As we know, the nonlinear coupling coefficient is related to the nonlinear susceptibility, and the longitudinal detuning function is related to the linear susceptibility, which can be expressed through Eqs. (2) and (3) below:

$$\chi_{as}^{(3)} = \frac{-N\mu_{20}\mu_{31}\mu_{21}\mu_{30}}{\varepsilon_0\hbar^3(\Delta_p + i\gamma_{02})(\delta - \Omega_e/2 + i\gamma_e)(\delta + \Omega_e/2 + i\gamma_e)}, \tag{2}$$

where μ_{ij} are the electric dipole matrix elements, and γ_{ij} is the dephasing rates. Δ_p is the pump-laser detuning and is defined as $\Delta_p = \omega_{20} - \omega_p$, N is the atomic density, $\Omega_e = [\Omega_c^2 - (\gamma_{30} - \gamma_{10})^2]^{1/2}$ is the effective coupling Rabi frequency, $\Omega_c = \mu_{24}E_c/\hbar$ is the coupling-laser Rabi frequency, γ_{10} and γ_{30} are the dephasing rates of coherence $|1\rangle \rightarrow |0\rangle$ and $|3\rangle \rightarrow |0\rangle$, $\gamma_e = (\gamma_{10} + \gamma_{30})/2$ is the effective dephasing rate, ε_0 is the permittivity of vacuum, and δ is resonance linewidth.

The linear susceptibility corresponding to the anti-Stokes is

$$\chi_{as} = \frac{N\mu_{30}^2}{\varepsilon_0\hbar} \frac{4(\Delta_c - \delta + \mathrm{i}\gamma_{01})}{4(\Delta_c - \delta + \mathrm{i}\gamma_{01})(\Delta_c - \delta + \mathrm{i}\gamma_{13}) - |\Omega_c|^2}, \tag{3}$$

where N is the atomic density, Δ_c is the coupling-laser detuning and is defined as $\Delta_c = \omega_{13} - \omega_c$, μ_{30} is the electric-dipole matrix elements, γ_{ij} are the dephasing rates, and δ is the resonance linewidth.

When the pump field E_p and coupling field E_c are kept constant, and the dressing laser having angular frequency ω_3 is applied to the quantum transition $|1\rangle \rightarrow |3\rangle$ with a detuning $\Delta_3 = \omega_{13} - \omega_3$, the dressing third-order nonlinear susceptibility tensor and linear susceptibility for the generated anti-Stokes field of Eqs. (2) and (3) can be rewritten as Eqs. (4) and (5), respectively:

$$\chi_{as}^{(3)} = -\frac{N\mu_{30}\mu_{20}\mu_{31}\mu_{21}}{\varepsilon_0\hbar^3(\Delta_p - i\gamma_{20})D_1(\delta)}, \tag{4}$$

$$\chi_{as} = \frac{N\mu_{30}^2}{\varepsilon_0\hbar} \frac{1}{\left[\frac{|\Omega_3|^2}{4(\delta+\Delta_3+\mathrm{i}\gamma_{13})} + \frac{|\Omega_c|^2}{4(\delta+\mathrm{i}\gamma_{13})} - (\delta + \mathrm{i}\gamma_{01})\right]}, \tag{5}$$

where $D_1(\delta)$ is defined as $D_1(\delta) = -4(\delta + \Delta_3 + i\gamma_{13})(\delta + i\gamma_{01})(\delta + i\gamma_{03}) + |\Omega_3|^2(\delta + i\gamma_{01}) + |\Omega_c|^2(\delta + \Delta_3 + i\gamma_{13})$, μ_{ij} are the electric-dipole matrix elements, γ_{ij} are the dephasing rates, $\hbar$ is Planck constant divided by 2π, ε_0 is the permittivity of vacuum, Ω_3 is the dressing Rabi frequency, and Δ_3 is the dressing-laser detuning from the atomic transition $|5S_{1/2}, F = 3\rangle \rightarrow |5P_{3/2}, F = 2\rangle$.

From Eq. (4), we can calculate the dressing effective Rabi frequency as

$$\Omega_e = \tfrac{1}{2}\left\{\Delta_3 \pm \left[4\Omega_3^2 + \Delta_3^2 - \left(\gamma_{10}^2 - \gamma_{30}^2\right)\right]^{1/2}\right\}$$

and the effective dephasing rate as

$$\gamma_e = \frac{2\Omega_3^2}{\Omega_e^2}\left(\frac{\gamma_{10} + \gamma_{13}}{2}\right) + \frac{\Delta_3^2}{\Omega_e^2}\gamma_{10}.$$

According to Wen and Du's theoretical analysis [27], there are three characteristic frequencies that principally determine the shape of the biphoton wave function. The first is the Rabi time $2\pi/\Omega_e$, which determines the two-resonance spectrum of the nonlinear susceptibility. The second is the linewidth

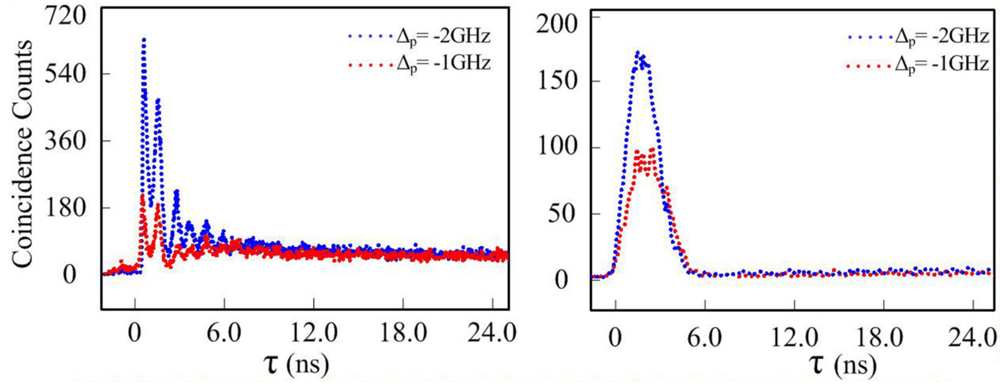

FIG. 2. Two-photon coincidence counts as a function of relative time delay τ between paired Stokes and anti-Stokes photons. The bin width is 0.0244 ns. (a) Biphoton generation at OD = 0.7, $P_c = 38$ mW, $P_p = 6$ mW, $\Delta_c = 1$ GHz. (b) Biphoton generation at OD = 0.7, $P_c = 20$ mW, $P_p = 6$ mW, $\Delta_c = 1$ GHz.

$2\gamma_e$ of the two resonances in the nonlinear susceptibility. The third is the full width at half maximum (FWHM) phase-matched bandwidth determined by the sinc function, $\Delta\omega_g = 2\pi \times 0.88/\tau_g$, where τ_g is the anti-Stokes group delay time. An experimental study of the dressing effect as a function of these three characteristic frequencies is warranted.

III. EXPERIMENTAL RESULTS

Figure 2 shows the no-dressing experimental results at an optical depth of 0.7. The coincidence counts exhibit damped Rabi oscillations due to the interference between two types of FWM processes [28]. In Figs. 2(a) and 2(b), at $\tau = 0$, $G^{(2)}$ has a sharp rise and then as $\tau \to \infty$, $G^{(2)}$ approaches zero, indicating the anti-bunching-like effect. In Fig. 2(a), the Rabi oscillations can be clearly observed with a period of about 1.1 ns, while in Fig. 2(b), we can only observe one oscillation period, noting that the experimental conditions of Figs. 2(a) and 2(b) are the same, except the coupling laser power P_c of Fig. 2(b) is reduced from 38 to 20 mW. Both Figs. 2(a) and 2(b) have a same correlation time of about 6 ns. The biphoton noise contrast ratio greatly increases by increasing the pumping detuning from −1 to −2 GHz, which is due to the reduction of accidental coincidence counts. The Rabi oscillations of biphoton waveforms in Figs. 2(a) exhibit a beat indicating the presence of more than one frequency. This is because that the coupling-laser Rabi frequency in Eq. (2) has multiple values that depend on the Clebsch–Gordan coefficients for the Zeeman level combinations with a given linearly polarization light [29]. This may give rise to additional $\chi_{as}^{(3)}$ resonances in Eq. (2) and enrich the oscillation period of the biphoton waveform.

According to the theory of Du *et al.* [27], the damped Rabi oscillation regime requires that the effective coupling Rabi frequency Ω_e and linewidth γ_e be smaller than the phase-matching bandwidth $\Delta\omega_g$. Under this condition, the optical properties of the two-photon amplitude $\psi(\tau)$ represented by Eq. (1) are mainly determined by the nonlinear coupling coefficient $\kappa(\omega_{as})$, which is proportional to the third-order nonlinear susceptibility $\chi_{as}^{(3)}$ as in Eq. (2). The damping rate is determined by the resonant linewidth γ_e in the doublet. In Fig. 2(b), the coupling-field effective Rabi frequency $\Omega_e = [\Omega_c^2 - (\gamma_{13} - \gamma_{12})^2]^{1/2}$ decreases with decreasing coupling-laser power. In the time domain this causes the Rabi time ($\tau_r = 2\pi/\Omega_e$) to be greater than the nonlinear coherence time ($\tau_e = 1/2\gamma_e$); that is, $\tau_r > \tau_e$. Consequently, the second and subsequent oscillations are all suppressed due to the short dephasing time, and only one oscillation period is observed in Fig. 2(b).

To characterize the nonclassical properties of our prepared biphoton, we obtain a violation of the Cauchy–Schwartz inequality $[g_{s,as}^{(2)}(\tau)]^2/[g_{s,s}^{(2)}(0)g_{as,as}^{(2)}(0)] \leqslant 1$ by factors of 16.20 and 23.6, respectively, for Figs. 2(a) and 2(b) (blue lines). These results verify the nonclassical nature of the entangled photons.

An objective of this work is to verify the relation between the dressing-laser detuning and the length of the biphoton waveform. In this section, we apply the dressing laser to the current energy conformation and fix the pump-laser power at 6 mW, the coupling-laser power at 38 mW, and the dressing-laser power at 9 mW, and vary the dressing-laser detuning, which is 1.0, 0.5, and 0 GHz for Figs. 3(a)–3(c), respectively. As expected, the two-photon correlation time becomes longer as we reduce the dressing-laser detuning for narrower linewidth. Figures 3(a)–3(c) show the biphoton coincidence results of beating (or interference) between multiple types of FWM processes. The physics behind this can be explained from the dressing third-order nonlinear susceptibility of Eq. (4). Solving the cubic function $\mathrm{Re}D_1(\delta) = 0$ in Eq. (4), where $D_1(\omega) = -4(\delta + \Delta_3 + i\gamma_{13})(\delta + i\gamma_{01})(\delta + i\gamma_{03}) + |\Omega_3|^2(\delta + i\gamma_{01}) + |\Omega_c|^2(\delta + \Delta_3 + i\gamma_{13})$, one can find three roots which indicate a triplet of resonances. The roots are $\delta = 0$, $\delta_\pm = (-\Delta_3 \pm \Omega_e')/2$, where $\Omega_e' = [\Delta_3^2 + |\Omega_3|^2 + |\Omega_c|^2 + 4(\gamma_{01}\gamma_{03} + \gamma_{01}\gamma_{13} + \gamma_{03}\gamma_{13})]^{1/2}$. It indicates that there are three types of FWM behind $D_1(\delta)$. The destructive interference caused by these three types of FWM results in beating in the two-photon waveform. The corresponding linewidths of this triplet of resonances are $\Gamma_0 = \gamma_{10}$, $\Gamma_\pm = [(\gamma_{01} + \gamma_{03})/2] \pm \Delta_3(\gamma_{01} - \gamma_{03})/\{2[|\Omega_3|^2 + \Delta_3^2 + 4\gamma_{01}\gamma_{03}]^{1/2}\}$. On the other hand, the electric dipole μ_{ij} which determines the coupling-laser Rabi frequency can be can be multi-valued in Eq. (4) because different combinations of the ground- and excited-state Zeeman levels that can be coupled with linearly polarized light [29], this may give rise to additional $\chi_{as}^{(3)}$ resonances and richer a richer spectrum of Rabi frequencies. The biphoton

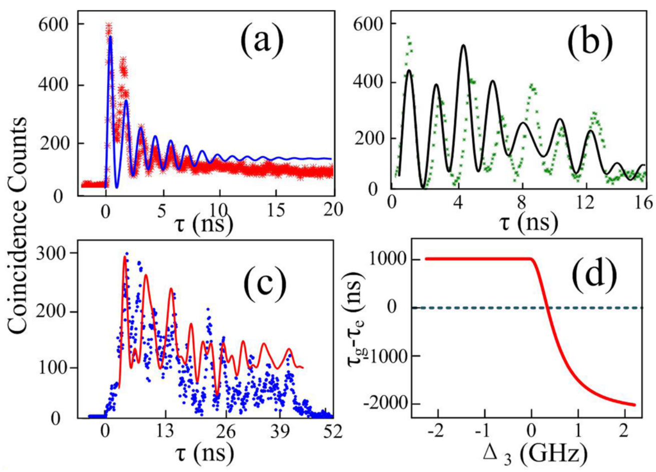

FIG. 3. (a)–(c) Changes of biphoton waveform with dressing-field detuning Δ_3. Two-photon coincidence counts, collected over 400 s with 0.0244 ns bin width as a function of the relative time delay τ between paired Stokes and anti-Stokes photons. The dressing frequency detuning for panels (a)–(c) are 1.0, 0.5, and 0 GHz, respectively. The solid line is the theoretical curve. (d) Theoretically simulation of difference between τ_g and τ_e as a function of dressing detuning Δ_3.

correlation time is determined by the resonance linewidths, which is related to dressing-laser detuning. Thus, the biphoton correlation time of Fig. 3(c) is prolonged by a change in the detuning of the dressing laser.

In addition, can the biphoton waveform transform from the Rabi-oscillation regime to the group-delay regime? In the following, we make predictions based on theory. The difference in group delay time is

$$\tau_g = \frac{L}{c}\left\{1+\frac{\omega_{31}}{2}\frac{N\mu_{13}^2}{\varepsilon_0\hbar}\frac{[\Delta_c(\Delta_c+\Delta_3)]}{(\Delta_c+\Delta_3)|\Omega_c|^2+\Delta_c|\Omega_3|^2}\right\},$$

and the nonlinear coherence time τ_e as a function of the dressing-frequency detuning has been simulated and is shown in Fig. 3(d). When $\Delta_3 > 0.5$ GHz, the calculated group-delay time τ_g is less than the nonlinear coherence time $\tau_e(\tau_g < \tau_e)$. Under these conditions, the Rabi-oscillation regime dominates the system behavior. When Δ_3 is tuned in the range of $0 < 0.5$ GHz, the group-delay time τ_g continues to increase and reaches a maximum value at $\Delta_3 = 0$ GHz. When $\Delta_3 <$ 0 GHz, the difference between τ_g and τ_e approaches a constant value, and in this condition ($\tau_g > \tau_e$), the group delay regime dominates the system behavior. In brief, the competition between τ_e and τ_g will determine which effect plays a dominant role in governing the features of the two-photon correlation.

As we know, the two-photon wave function is a convolution of the nonlinear and linear optical responses [27]. According to this convolution, the two-photon temporal correlation is considered in two regimes: damped Rabi oscillation and group delay. In Fig. 3, we focused on controlling the biphoton waveform by changing the dressing-laser detuning in the damped Rabi-oscillation regime. In this section, we mainly focus on the group delay regime by varying the power of the dressing laser. The rubidium vapor cell temperature is raised to 110 °C (optical density =2.99) and the dressing-laser detuning Δ_3 is fixed at −1.0 GHz according to the results of Fig. 3. Based on these conditions, and by optimizing the dressing-field power to 4 mW, we achieve a near "rectangle" shape with a correlation time of 165 ns, as seen in Fig. 4(a). The physics behind this is that dressing laser has a modulation effect on the Rb vapor

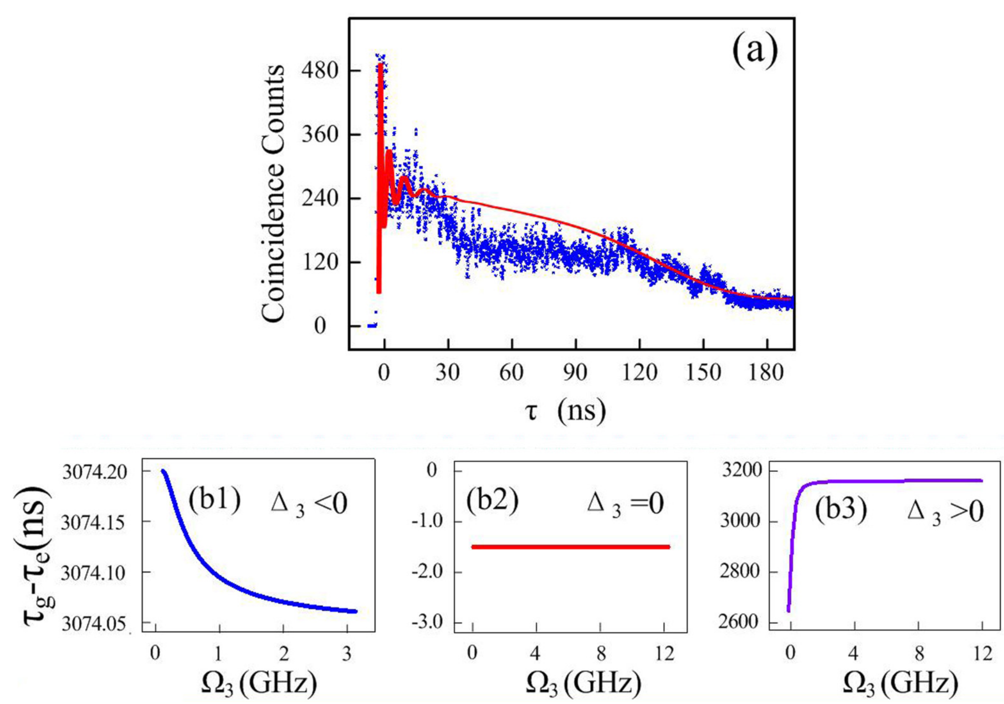

FIG. 4. (a) Two-photon coincidence counts as a function of relative time delay τ between paired Stokes and anti-Stokes photons collected over 1000 s with 0.0244 ns bin width. The dressing-field power is 4 mW, and the Rb temperature is 110 °C. The red line is the theoretical curve. (b1)–(b3) Theoretically simulated difference between τ_g and τ_e as a function of dressing Rabi frequency Ω_3.

cell energy level. In our four-energy-level system, the energy level $|3\rangle$ is first split into $\lambda_\pm$ by the coupling laser $\boldsymbol{E}_1$. The λ_+ energy level then experiences a second-order splitting into λ_{++} and λ_{+-} by the dressing laser $\boldsymbol{E}_3$. As a consequence, the EIT effect obtained in the current configuration is manipulated by both the Rabi frequency of the coupling laser and the dressing laser. As suggested by Balic *et al.* [30] and Kolchin [31] and demonstrated by Du *et al.* [17], the group-delay regime is defined as $\tau_g > \tau_r$ and the EIT and slow-light effects can be used to dynamically control the biphoton temporal correlation time. From the anti-Stokes photons' group delay time τ_g, which is defined as

$$\tau_g = \frac{L}{c}\left\{1+\frac{\omega_{31}}{2}\frac{N\mu_{13}^2}{\varepsilon_0\hbar}\frac{[\Delta_c(\Delta_c+\Delta_3)]}{(\Delta_c+\Delta_3)|\Omega_c|^2+\Delta_c|\Omega_3|^2}\right\},$$

we also get that the biphoton correlation time is related to both the dressing laser and the coupling laser Rabi frequency. The theoretical photon pair generation rate under the group-delay regime is $R = |\kappa_0|^2 V_g L$, which is similar to conventional SPDC photons with a rectangular-shaped biphoton wave packet [32]. Here, the nonlinear coupling coefficient κ_0 is treated as a constant over the phase-matching spectrum. The anti-Stokes photons' group velocity is defined as

$$V_g = c\Bigg/\left\{1+\frac{\omega_{31}}{2}\frac{N\mu_{13}^2}{\varepsilon_0\hbar}\frac{4[\Delta_c(\Delta_c+\Delta_3)]}{(\Delta_c+\Delta_3)|\Omega_c|^2+\Delta_c|\Omega_3|^2}\right\}.$$

An exponential-decay behavior in the tail of biphoton waveform is due to the finite EIT loss, which alters the correlation function shape, which deviates away from the ideal rectangular shape. There is a sharp peak at the leading edge of the biphoton waveform, which is the so called optical precursor [33]. This phenomenon requires that the simultaneously generated Stokes and anti-Stokes photons travel near the speed of light in vacuum and arrive near-simultaneously at the photodetectors [34]. Figures 4(b1)–4(b3) show the theoretical curve of the difference between group-delay time τ_g and nonlinear coherence time τ_e as a function of the dressing Rabi frequency. The group-delay condition is equivalent to $\tau_g > \tau_e$; one can achieve a system dominated by group-delay regime at $\Delta_3 < 0$ or $\Delta_3 > 0$ by varying the dressing-laser Rabi frequency. If the dressing detuning is at resonance (i.e., $\Delta_3 = 0$), the group-delay time τ_g is always less than nonlinear coherence time τ_e with the variation in dressing Rabi frequency, which means that the system is dominated by the nonlinear-Rabi-oscillation regime. One cannot achieve a biphoton waveform with a "rectangle" shape under these conditions.

IV. CONCLUSION

In conclusion, in a four-energy-level system, we have used hot atomic-gas media to generate nonclassical light through the SFWM process, specifically focusing on narrowband biphoton generation. By controlling the dressing-laser detuning and power, the biphoton correlation time is prolonged and the waveform changes. We also observed Rabi oscillations and optical precursors in hot atoms. The effect of the dressing laser on the competition between the processes of group-delay time and nonlinear coherence time is analyzed in detail. In future work, based on the dressing effect, accompanied by optimum coupling field power and detuning, and optical pumping field [24], the biphoton correlation time can be made more tunable. This work has potential practical applications in quantum optics.

ACKNOWLEDGMENTS

This work was supported by the National Key R&D Program of China (Grant No. 2017YFA0303700), the National Nature Science Foundation of China (Grants No. 11474228 and No. 11604256), the Key Scientific and Technological Innovation Team of Shaanxi Province (Grant No.2014KCT-10), and the Natural Science Foundation of Shaanxi Province (Grant No. 2015JQ6233) and the Fundamental Research Funds for the Central Universities (Grant No. xjj2016030).

[1] A. Einstein, B. Podolsky, and N. Rosen, Phys. Rev. **47**, 777 (1935).
[2] T. B. Pittman, Y. H. Shih, D. V. Strekalov, and A. V. Sergienko, Phys. Rev. A **52**, R3429 (1995).
[3] D. V. Strekalov, A. V. Sergienko, D. N. Klyshko, and Y. H. Shih, Phys. Rev. Lett. **74**, 3600 (1995).
[4] L. Duan, M. D. Lukin, J. I. Cirac, and P. Zoller, Nature (London) **414**, 413 (2001).
[5] C. Weedbrook, S. Pirandola, R. Garciapatron, N. J. Cerf, T. C. Ralph, J. H. Shapiro, and S. Lloyd, Rev. Mod. Phys. **84**, 621 (2012).
[6] P. G. Kwiat, K. Mattle, H. Weinfurter, A. Zeilinger, A. V. Sergienko, and Y. Shih, Phys. Rev. Lett. **75**, 4337 (1995).
[7] C. Simon, H. de Riedmatten, M. Afzelius, N. Sangouard, H. Zbinden, and N. Gisin, Phys. Rev. Lett. **98**, 190503 (2007).
[8] Z. Y. Ou and Y. J. Lu, Phys. Rev. Lett. **83**, 2556 (1999).
[9] X.-H. Bao, Y. Qian, J. Yang, H. Zhang, Z.-B. Chen, T. Yang, and J. W. Pan, Phys. Rev. Lett. **101**, 190501 (2008).
[10] J. Fekete, D. Rielander, M. Cristiani, and H. de Riedmatten, Phys. Rev. Lett. **110**, 220502 (2013).
[11] M. Förtsch, J. U. Fürst, C. Wittmann, D. Strekalov, A. Aiello, M. V. Chekhova, C. Silberhorn, G. Leuchs, and C. Marquardt. Nat. Commun. **4**, 1818 (2013).
[12] G. Schunk, U. Vogl, D. V. Strekalov, M. Fortsch, F. Sedlmeir, H. G. L. Schwefel, M. Gobelt, S. Christiansen, G. Leuchs, and C. Marquardt, Optica **2**, 773 (2015).
[13] G. Schunk, U. Vogl, F. Sedlmeir, D. V. Strekalov, A. Otterpohl, V. Averchenko, H. G. L. Schwefel, G. Leuchs, and Ch. Marquardt, J. Mod. Opt. **63**, 2058 (2016).
[14] H. Zhang, X. M. Jin, H. N. Dai, S. J. Yang, and T. M. Zhao, Nat. Photon. **5**, 628 (2011).
[15] S. V. Polyakov, C. W. Chou, D. Felinto, and H. J. Kimble, Phys. Rev. Lett. **93**, 263601 (2004).
[16] H. Xia, S. J. Sharpe, A. J. Merriam, and S. E. Harris, Phys. Rev. A **56**, R3362 (1997).
[17] S. Du, P. Kolchin, C. Belthangady, G. Y. Yin, and S. E. Harris, Phys. Rev. Lett. **100**, 183603 (2008).
[18] C. Liu, L. Zhao, M. M. T. Loy, X. Guo, S. Du, and Y. Sun, Optica **1**, 84 (2014).

[19] Z. Han, P. Qian, L. Zhou, J. F. Chen, and W. Zhang, Sci. Rep. **5**, 9126 (2015).
[20] L. Zhao, X. Guo, Y. Sun, Y. Su, M. M. T. Loy, and S. Du, Phys. Rev. Lett. **115**, 193601 (2015).
[21] J. F. Chen, S. Zhang, H. Yan, M. M. T. Loy, G. K. L. Wong, and S. Du, Phys. Rev. Lett. **104**, 183604 (2010).
[22] S. Zhang, J. F. Chen, C. Liu, S. Zhou, M. M. T. Loy, and G. K. Wong, Rev. Sci. Instrum. **83**, 073102(2012).
[23] M. D. Eisaman, L. Childress, A. Andre, F. Massou, A. S. Zibrov, and M. D. Lukin, Phys. Rev. Lett. **93**, 233602, (2004).
[24] C. Shu, P. Chen, T. K. A. Chow, L. Zhu, Y. Xiao, M. M. T. Loy, and S. Du, Nat. Commun. **7**, 12783 (2016).
[25] L. Zhu, X. Guo, C. Shu, H. Jeong and S. Du, Appl. Phys. Lett. **110**, 161101 (2017).
[26] J. M. Wen and M. H. Rubin, Phys. Rev. A **74**, 023808 (2006).
[27] S. Du, J. M. Wen, and M. H. Rubin, J. Opt. Soc. Am. B **25**, C98 (2008).
[28] H. Yan, S. Zhang, J. F. Chen, M. M. T. Loy, G. K. L. Wong, and S. Du, Phys. Rev. Lett. **106**, 033601 (2011).
[29] P. J. Ungar, D. S. Weiss, E. Riis, and S. Chu, J. Opt. Soc. Am. B **6**, 2058 (1989).
[30] V. Balic, D. A. Braje, P. Kolchin, G. Y. Yin, and S. E. Harris, Phys. Rev. Lett. **94**, 183601 (2005).
[31] P. Kolchin, Phys. Rev. A **75**, 033814 (2007).
[32] A. V. Sergienko, Y. H. Shih, and M. H. Rubin, J. Opt. Soc. Am. B **12**, 859 (1994).
[33] S. Zhang, J. F. Chen, C. Liu, M. M. T. Loy, G. K. L. Wong, and S. Du, Phys. Rev. Lett. **106**, 243602 (2011).
[34] H. Jeong, A. M. Dawes, and D. J. Gauthier, Phys. Rev. Lett. **96**, 143901 (2006).